2026 S.T. Yau High School Science Award (Asia)

Research Report

The Team

Registration Number: Physics-226

Name of team member: Arjun Mehrotra
School: Ascend International School
Country: India

Name of supervising teacher: Craig Lancaster Marr
Job Title: Academic Research Librarian
School: Ascend International School
Country: India

Chaos Analysis in Systems of Non-Linearly Coupled Magnetic Pendula

Date

17 August 2026

2026 S.-T. Yau High School Science Award
仅用于2026丘成桐中学科学奖论文公示

Chaos Analysis in Systems of Non-Linearly Coupled Magnetic Pendula

Arjun Mehrotra

Abstract

We study a system of repelling magnets arranged in the shape of a Newton's cradle. While the system's behavior is easy to observe, the coupling is strongly nonlinear. The transition from regular motion to chaos in such a chain has not to our knowledge previously been characterized as a coupled-oscillator system. This work analyzed both regimes. The coupling is built from the Furlani force, and from this the system's normal modes are derived and tested. We build a novel and highly precise experimental setup that allows us to independently vary spacing, length, and magnet remanence, and use automated tracking to reduce errors. At large amplitudes, chaos is confirmed first qualitatively through phase-space portraits, and then through the determination of the Maximum Lyapunov Exponent (MLE), which we compute both theoretically and experimentally. We show that the degree of chaos in the system increases with the chain strength. More broadly, this system serves a useful test in which coupling strength and size are directly tunable, thereby making it a more general model for the onset of chaos in coupled non-linear lattices of any kind.

Keywords: chaos theory, magnetic coupling, non-linear oscillations, normal modes, Lyapunov exponent

2026 S.-T. Yau High School Science Award
仅用于2026丘成桐中学科学奖公示

Acknowledgement

I would like to thank Mr. Craig Lancaster Marr for his constant support throughout the entire research process. I would also like to thank Ms. Tina Jain for her support with my physics questions and experimentation. This report would not be possible without their guidance and advice on best practices.

2026 S.-T. Yau High School Science Award
仅用于2026丘成桐中学科学奖论文公示

Research Report 2026 S.T. Yau High School Science Award (Asia)

Commitments on Academic Honesty and Integrity

We hereby declare that we

1. are fully committed to the principle of honesty, integrity and fair play throughout the competition.
2. perform the research work ourselves and thus truly understand the content of the work.
3. observe the common standard of academic integrity adopted by most journals and degree theses.
4. have declared all the assistance and contribution we have received from any personnel, agency, institution, etc. for the research work.
5. have truthfully disclosed all AI tool usage in the research report and obtained prior approval from supervising teachers. All supporting documentation has been submitted as required. We hereby affirm that no improper use of AI has occurred at any stage of the research process.
6. undertake to avoid getting in touch with assessment panel members in a way that may lead to direct or indirect conflict of interest.
7. undertake to avoid any interaction with assessment panel members that would undermine the neutrality of the panel member and fairness of the assessment process.
8. observe the safety regulations of the venue(s) where we conduct the experiment(s), if applicable.
9. observe all rules and regulations of the competition.
10. agree that the decision of YHSA(Asia) is final in all matters related to the competition.

We acknowledge that this work was previously submitted to the Indian Young Physicists' Tournament (InYPT) and thereafter to the International Young Physicists' Tournament (IYPT).

We understand and agree that failure to honor the above commitments may lead to disqualification from the competition and/or removal of award, if applicable; that any unethical deeds, if found, will be disclosed to the school principal of the team member(s) and relevant parties if deemed necessary; and that the decision of YHSA(Asia) is final and no appeal will be accepted.

Name of team member: Arjun Mehrotra

X

Name of supervising teacher:

Noted and endorsed by

(signature)

Name of school principal:

2026 S.T. Yau High School Science Award
仅用于2026丘成桐中学科学奖论文公示

Table of Contents

Abstract i

Acknowledgement ii

Commitments on Academic Honesty and Integrity iii

1. Introduction 6
2. Literature Review 7
3. Methodology 8
4. Results 19
5. Limitations and Future Scope 25
6. Conclusion 25
7. References 26
8. Appendix 27

2026 S.-T. Yau High School Science Award
仅用于2026丘成桐中学科学奖论文公示

1 Introduction

The problem “Magnetic Newton’s Cradle”, first introduced in the IYPT 2026, concerns itself with the motion of a system of magnetic pendula under different conditions. Much like a mechanical newton’s cradle, which

demonstrates momentum transfer and inelastic collisions, the Magnetic Newton's cradle demonstrates the concepts of coupled oscillations and non-linear behavior. Each pendulum carries a magnet, and neighboring magnets repel each other, thus transferring energy through non-contact force.

At small displacements, we see that the pendula settle into specific normal modes. We observe the symmetric modes, where all magnets move in phase (including the centrosymmetric modes where the middle magnet moves very little) and the antisymmetric modes, where certain magnets move out of phase. At larger displacements, magnetic repulsion becomes more important, and the coupling effects become highly non-linear. Unlike the mechanical newton's cradle which displays the same behavior for any number of bobs, this magnetic system varies based on the number of magnets, and the present work aims to investigate this.

We make certain novel contributions in our study of this system. Firstly, we treat the magnetic cradle as a one dimensional coupled oscillator chain, and deriving its normal modes. Secondly, we introduce a coupling matrix which uses the Furlani force instead of the dipole approximation. Thirdly, we quantify the systems descent into chaos as the number of magnets changes, using the Lyapunov exponent on both experimental and numerically integrated trajectories. Our most important contribution is that of a highly reproducible and robust experimental setup, with 3D printed components allowing for the variation of many parameters and automated tracking to reduce experimental error.

These results can have impacts on the study of more general coupled chains of oscillators, especially in areas like lattice dynamics and arrays of resonators. Our study of the chaotic and modal behavior of the system is highly controlled and precise, and therefore serves a powerful physical test of how coupling strength and tunable parameters drive transitions into chaos.

2026 S.-T. Yau High School Science Award
仅用于2026丘成桐中学科学奖公示

2 Literature Review

The canonical entry point for mechanical chaos is the double pendulum. Shinbrot et al. [3] measured the exponential separation of nearby trajectories in a physical double pendulum and recovered a positive Lyapunov exponent. This established a deterministic system with only two coupled degrees of freedom is sufficient to produce sensitive dependence on initial conditions. Strogatz [8] pioneered much of the mathematical underpinning of chaos. He framed phase-space portraits as qualitatively separating regular from aperiodic motion. He also described the largest Lyapunov exponent as the quantitative way of discriminating them.

In literature, magnetic coupling has been studied primarily through basins of attraction. Peitgen et al. [9] give the classic model of a bob swinging over magnets fixed at the vertices of a triangle and studied it through fractals. Building on this, the work in [10] implemented a more physical magnetic-interaction model and found fractal structure in the basin boundaries. Most directly relevant, work in [11] constructed a variable-distance magnetic pendulum, tracked its trajectories experimentally, and used a heat map of Lyapunov exponent to correlate coupling strength with the degree of chaos. However, all three works treat a two-dimensional magnet-versus-magnet interaction, and none analyze a one-dimensional chain of pivoted magnets as a coupled-oscillator system. This is the gap that the present work aims to address.

For the magnetic force model, the point-dipole approximation is the standard approach, but it breaks down as the distance between magnets approaches the magnet diameter. For close range, the bound surface-current (Ampèrian) model replaces magnetization with currents evaluated by Biot–Savart. Ravaud et al. [5] established the equivalence of this current model and the Coulombian charge model. Vučković et al. [6] applied the surface-current formulation to compute interaction forces efficiently. Furlani [4] treats the force between two coaxial disks as the sum of Coulomb interactions between their four faces, which helps us avoid the dipole model. This study builds on both branches, using the surface-current model for the general numerical torque and the Furlani form for the linearized modal analysis.

The small-amplitude behavior is dependent on the theory of coupled linear oscillators. Georgi [14] and Cline [15] develop the normal-mode formalism including the cutoff behavior that appears when coupling is short-range. Spectral identification of these modes relies on the fast Fourier transform of Cooley et al. [13].

Savitzky et al. [2] introduced the least-squares polynomial filter applied here to the tracked angle signal, reducing noise and increasing data fidelity. Rosenstein et al. [1] developed the algorithm used to extract the Lyapunov exponent from experimental time series, and it is robust to embedding dimension, data-set size, and noise. Trajectory extraction itself uses the OpenCV library [12] for per-magnet center-of-mass tracking. Taken together, the prior literature has studied magnetic forces and chaotic systems to some extent, and the contribution of this work is to combine them on a single physical chain.

2026 S.T. Yau High School Science Award 仅用于2026丘成桐中学科学奖公示

3 Methodology

3.1 Experimental Setup

3.1.1 Frame and Magnets

The supporting structure is a 3D-printed rectangular frame with a row of evenly spaced hole along the top. Each magnetic carrier is 3D-printed, with measurements taken for the diameter of the magnets to ensure enough space. The pendula pivot on wooden dowels that are placed in these holes, and thus the horizontal spacing between adjacent pendula is easily variable.

Each pendulum arm is a 3D-printed bifilar carrier holding a disk magnet at its lower end. The carrier has its own row of holes along the arm, which allows us to vary the effective pendulum length. This gives us two variable parameters - l, the length of the pendulum arm, and d, the distance from the pivot to the center of mass of the magnet.



Fig. 1 – Experimental Setup

The interacting elements are disk-shaped neodymium magnets, of which we use four grades: N35, N38, N40, and N42. These 4 magnets have identical diameters and thickness, and vary only in remanent magnetization. The magnet's remanence is calibrated directly against a Vernier magnetic field sensor, and cross-checked with the values from the manufacturer.

The 3-D printed carriers are displayed here:

2026 S.T. Yau High School Science Award
仅用于2026年度获奖论文公示

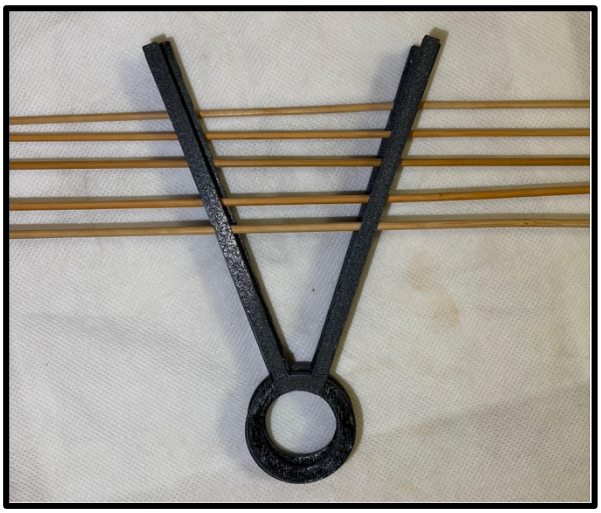


Fig. 2 – 3D printed magnets with Axles

Some relevant parameters of the system are shown below:

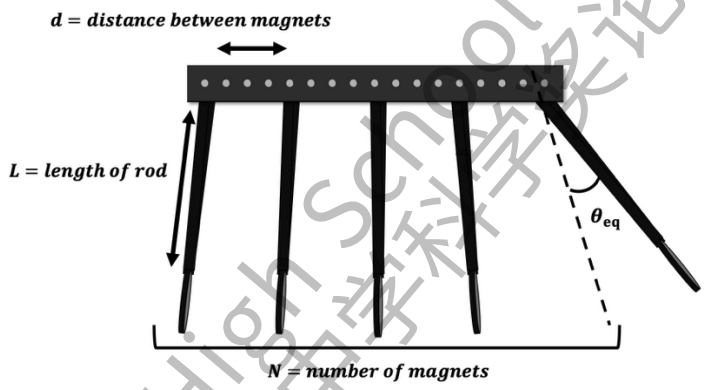


Fig. 3 – Relevant parameters

3.1.2 Imaging

The motion of the system is recorded with a tripod-mounted camera at 240 frames per second. The high frame rate is required because the higher modes reach angular frequencies of many hertz. Therefore, we must use a slow-motion camera to ensure adequate resolution. A ruler is placed in the plane of motion for calibration.

We extract angles from the raw footage using OpenCV to track the center of mass of each magnet over time. This allows us to detect every magnet individually in a highly reproducible manner. Before we use the experimental signal, we take the Savitsky-Golay filter on the data, which fits a low-order polynomial and reduces noise. Secondly, we correct parallax by computing a homography between fixed points on the frame of the cradle relative to the camera, which brings our error in the angle down to $\pm 2.34°$.

2026 S.T. Yau High School Science Award
仅用于2026丘成桐中学科学奖论文公示

This automated system therefore allows us to extract highly usable data from an experimental setup that allows for variability, giving us an output of angle over time for each magnetic carrier.

3.2 System Definition

3.2.1 Torques

The cradle is described in the fixed lab frame. The origin is placed at the pivot of the first pendulum, and the other pivots are evenly spaced afterwards:

$$\vec{P_j} = (a(j-1), 0)$$

Where a is the horizontal spacing between the holes (the minimum spacing is $a = 1\ cm$). For a system of N pendula, each magnet is assigned a generalized coordinate θ_j, so that the full configuration of the system at any point is given by the vector $[\theta_1, \theta_2, \dots, \theta_N]$.

The motion of each pendulum comes from newton's law of rotation about a fixed axis:

$$I\ddot{\theta}_j = \sum \tau_j$$

We sum up the torque on each pendulum acting due to gravity, the magnetic interaction between all N magnets, dry coulomb torque (which acts at the axle), and quadratic dissipative torque.

We therefore get:

$$I\ddot{\theta}_j = -\tau_{mag} - \tau_g - \tau_c sgn(\dot{\theta}) - C_d|\dot{\theta}|\dot{\theta}$$

Where $\tau_c sgn(\dot{\theta})$ is a constant opposing Coulomb torque due to friction between the wooden axle and the plastic frame. Noticing that the peak angular velocity of the magnet is roughly $3\frac{rad}{second}$, the Reynolds number for the system is on the order of $O(10^2)$, and we therefore not in the stokes regime. Therefore, we opt to use quadratic and not linear drag, where C_d represents a constant drag coefficient.

3.2.2 Damping Fit

Both C_d and τ_c are fitted using a single magnet case, where there is no magnetic torque and the only forces acting are the coloumb Force, gravitational Force, and air resistance.

2026 S.T. Yau High School Science Award 仅用于2026丘成桐中学科学奖论文公示

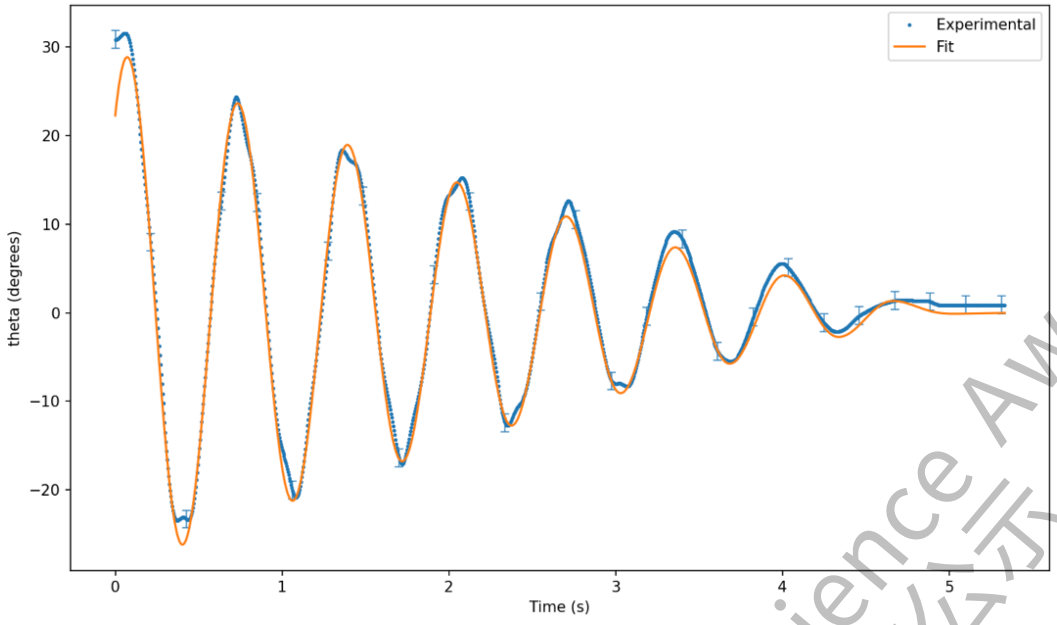


Fig. 4 – Damping Fit

Fitting the graph as shown gives the values of the normalized

$$\frac{C_d}{I} = 0.0883 \pm 0.0041 \frac{1}{rad \cdot s}$$

And

$$\frac{\tau_c}{I} = 1.203 \pm 0.017 \frac{rad}{s^2}$$

These values are used thereafter.

3.3 Rigid Body Analysis

3.3.1 Gravitational Torque

Because we are not assuming that the pendulum is idealized with all the mass at the center, the gravitational torque τ_g can be written as the sum of the gravitational torque acting at the magnetic bob plus the gravitational torque acting on both rods:

$$\tau_g = \tau_{g,bob} + \tau_{g,rods}$$

The torque acting due to the bob is simply

$$Mg \times d = Mgd\ sin(\theta_j)$$

Each arm is a rod of linear mass density μ. The mass of a small element at a distance x from the pivot is

2026 S.T. Yau High School Science Award
仅用于2026丘成桐中学科学奖论文公示

therefore:

$$dm = \mu\, dx$$

And the torque acting on it is:

$$d\tau = \mu g \cdot\ x \cdot \sin(\theta_j)\, dx$$

Integrating across the length of a rod and multiplying by two, we get:

$$\tau_{g,rods} = 2\int_0^l \mu g x \sin(\theta_j)\, dx$$

And thus the total gravitational torque is:

$$\tau_g = Mgd\sin(\theta_j) + 2\int_0^l \mu g x \sin(\theta_j)\, dx$$
$$= (Md + \mu l^2) g \sin(\theta_j)$$

Where:

- M = mass of the magnet
- d = distance from the pivot to the center of mass of the magnet
- l = length of each magnetic carrier
- μ = linear mass density of the carrier (found by taking mass of the carrier and dividing by length)
- θ_j = the instantaneous angle that carrier j makes with the vertical

3.3.2 Moment of inertia.

As with the gravitational torque, because are not assuming the pendulum to be an idealized mass, we must calculate the moment of inertia of both the magnets and the rods:

$$I_{total} = I_{magnet} + I_{rods}$$

Using the equation for the moment of inertia of a disk about its diameter and noticing that the distance between the magnets center of mass and the axis of rotation, the parallel axis theorem gives:

$$I_{magnet} = \frac{1}{4}Mr^2 + Md^2$$

Like before, we perform an integral over the length of the rod to get its moment of inertia:

$$I_{rods} = 2\int_0^l x^2\, dm = 2\int_0^l x^2\, \mu dx = \frac{2}{3}\mu l^3$$

2026 S.T. Yau High School Science Award
仅用于2026丘成桐中学科学奖论文公示

We thus get the moment of inertia to be:

$$I_{total} = M\left(\frac{1}{4}r^2 + d^2\right) + \frac{2}{3}\mu l^3$$

Where r is the radius of the magnet. Note that because d is on the order of 10 cm and r is on the order of 1 cm, $Md^2 \gg \frac{1}{4}Mr^2$ by about a factor of 100, and $\frac{1}{4}Mr^2$ can thus be neglected.

3.4 Magnetic Field Model

3.4.1 Surface Currents Model

The only term left in the equation of motion is τ_{mag}, which is the source of all the interactions between the pendula. In order to compute it we need to know the repulsive force between two magnets as a function of their separation and orientation, and this in turn requires knowing the magnetic field of the magnet.

The standard approximation for the field produced by two permanent magnets is the dipole model. However, the dipole model only holds for distances far larger than the sizes of the magnets. Because the magnets in our system sit close together, the dipole model does not work for this study.

Consequently, we use the bound surface currents model, assuming that its magnetization can be replaced by the surface currents around its rim [6].

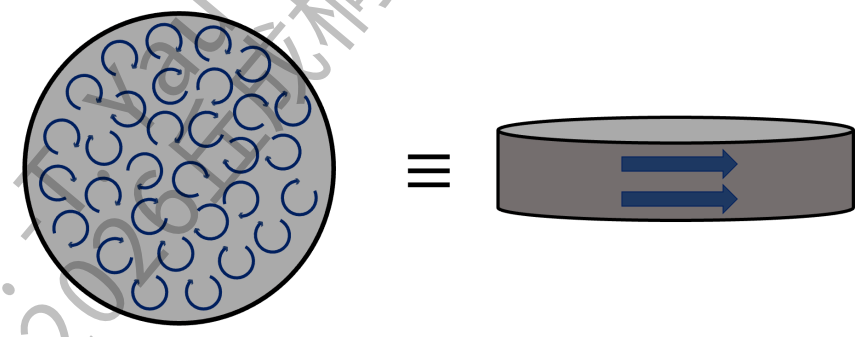


Fig. 5 – Surface Currents Model

The field of a source magnet at any point is obtained directly from Biot-Savart by integrating $d\vec{\boldsymbol{l}}$ around its rim loop:

$$B_r = \frac{\mu_0 I}{4\pi}\oint \frac{d\vec{l} \times (r - r')}{|r - r'|^3}$$

2026 S.T. Yau High School Science Award 仅用于2026丘成桐中学科学奖论文公示

Which represents the magnetic field at a point r from the surface rim element r'. Once we have computed the magnetic field, we can also find the Lorentz force on a target magnet which is also modelled with a certain field:

$$F_{mag} = I \iint d\vec{l} \times B_r$$

And finally, we get that the total magnetic torque acting on the magnet is given by:

$$\tau_{mag} = I \iint r' \times (d\vec{l} \times B_r)$$

The drawback of this method is that the magnetic torque must be calculated numerically, and this is computationally intensive.

3.4.2 Furlani Model

In order to get a closed form expression for the magnetic field, we use the Furlani model [4]. Furlani models the force between two coaxial and cylindrical magnets by treating the force between the two magnets as the sum of the Coloumb interactions between their four faces. Two of these pairs are between the faces with like charge and produce repulsion, while the other two are between opposite faces and produce attraction. Consequently, the Furlani model therefore does not have a simple $B_r \propto \frac{1}{r^4}$ scaling law like in the dipole model.

For two identical disks of radius R, thickness L, and remanent flux density B_r separated by a face-to-face gap x, the equation is given as:

$$Fur(x_{ij}) = \frac{\pi B_r^2 R^4}{4\mu_0}\left[\frac{1}{x^2} + \frac{1}{(x+2L)^2} - \frac{2}{(x+L)^2}\right]$$

In our cradle, the magnets are coaxial only when both pendula hang straight down, and we use it for small angles about the rest position. To apply this to our system we need the separation between each pari of magnets as a function of the pendulum angles. The center of magnet j is at:

$$\vec{r_j} = \vec{P_j} + l\begin{bmatrix}\sin(\theta_j)\\ -\cos(\theta_j)\end{bmatrix}$$

2026 S.-T. Yau High School Science Award 仅用于2026丘成桐中学科学奖论文公示

Where $\overrightarrow{P_j}$ is the pivot, and l is the arm length. For small angles, the face-to-face gap which is required for the Furlani force is:

$$x_{ij} \approx \left|\vec{r_j} - \vec{r_i}\right| - L$$

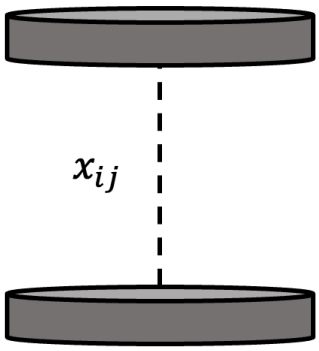


Fig. 6 – Furlani Face-to-Face distance

Then, the force on magnet j from magnet i acts along the line which joins both of their centers:

$$\overrightarrow{F_{ij}} = Fur(x_{ij})\,\widehat{n_{ij}}$$

And we can get an expression for the total torque acting on the jth magnet due to all the others:

$$\tau_{mag,\,j} = \sum_{i \neq j} \left[\left(\vec{r_i} - \vec{P_i}\right) \times \overrightarrow{F_{ij}}\right]$$

Because $Fur(x_{ij})$ is an explicit function of the angles through x_{ij}, the magnetic torque can now be differentiated in close form.

3.5 Modal Analysis

The central subject of this work is the chaotic motion of the coupled cradle. However, in the small amplitude limit, the overall chaotic motion of the cradle is not seen, and instead we see physically interpretable normal modes. In order to understand the underlying behavior of the cradle and what gives rise to chaos, we must therefore analyze the normal modes of the system.

At rest, the system sits as the equilibrium configuration $\theta_{eq} = [\theta_{eq,1}, \theta_{eq,2}, \ldots, \theta_{eq,N}]$. This occurs when the magnetic repulsion on each pendulum is exactly balances by gravity. We shall consider small perturbations from this configuration:

2026 S.T. Yau High School Science Award 仅用于2026丘成桐中学科学奖论文公示

$$\theta_j = \theta_{eq,j,} + x_j$$

Note that to find the normal modes, the quadratic drag and coloumb terms are dropped, as damping leads to negligible shifts in the frequency. Where x_j is the perturbation of pendulum j. The total torque on each pendulum is some function of all the angles in the system. For small x_j, we can take the first-order multivariable Taylor Expansion:

$$\tau_j(\theta_{eq} + x_j) \approx \tau_j(\theta_{eq}) + \sum_{k=1}^{N} \left.\frac{\partial \tau_j}{\partial \theta_k}\right|_{eq} x_k$$

At equilibrium, $\tau_j(\theta_{eq})$ = 0, and can thus be ignored. The coefficients

$$\tau_{jk} = \left.\frac{\partial \tau_j}{\partial \theta_k}\right|_{eq}$$

let us measure how strongly the displacement of pendulum k pushes on pendulum j. Hence, putting this back into the equation for torque and writing it in the rotational form yields a linear system:

$$\tau_j(\theta_{eq} + x_j) = \tau_j = I_j \ddot{x_j} = \sum_{k=1}^{N} \tau_{jk}\ x_k$$

Each τ_{jk} combines the sum of magnetic and gravitational components, which are differentiated to get:

$$\frac{\partial \tau_j}{\partial \theta_k} = \frac{\partial \tau_{mag,j}}{\partial \theta_k} - \delta_{j,k}\tau_g \cos(\theta_{j,eq})$$

Notice that the magnetic torque couples across all magnets in the row. The Kronecker delta is 1 if j and k are equal, and 0 otherwise. This simply encodes the fact that the gravitational torque on 1 magnetic carrier only impacts itself.

The linearized equations can be more easily represented in matrix form over all N magnet carriers:

$$\mathbf{M}\ddot{\mathbf{x}} = \mathbf{K}\mathbf{x}$$

Where M is the moment of inertia matrix:

2026 S.T. Yau High School Science Award 仅用于2026丘成桐中学科学奖论文公示

$$\mathbf{M} = \begin{bmatrix} I_1 & \cdots & 0 \\ \vdots & \ddots & \vdots \\ 0 & \cdots & I_N \end{bmatrix}$$

And K is the matrix of all the coupling coefficients τ_{jk}:

$$\mathbf{K} = \begin{bmatrix} \tau_{1,1} & \cdots & \tau_{1,N} \\ \vdots & \ddots & \vdots \\ \tau_{N,1} & \cdots & \tau_{N,N} \end{bmatrix}$$

This matrix clearly defines the coupling between any two matrices, encoding the restoring torque on pendulum j due to the displacement of pendulum k.

Noticing that all moments of inertia in this system are the same, we can divide through by $\boldsymbol{I_1 = I_2 = I_3 = \cdots = I_N = I}$ to get what we call the *normalized coupling matrix* A:

$$\mathrm{A} = \frac{\mathrm{K}}{\mathrm{I}}$$

Assuming that normal mode solutions where every pendulum oscillates at a common frequency ω exist, we can write:

$$\mathrm{x} = \psi e^{i\omega t}$$

Where the vector ψ holds the amplitude for every magnet in the pattern. Substituting this into the linear system gives:

$$\omega^2 \psi = \mathrm{A}\,\psi$$

The solution to this eigenvalue problem gives us the normal modes of the system.

The matrix A also has two interesting behaviors. Due to the Furlani model, it exhibits short-range coupling, and A is therefore a tridiagonal matrix where only its two-nearest neighbors contribute significantly.

2026 S.T. Yau High School Science Award
仅用于2026丘成桐中学科学奖论文公示

3.6 Numerical Integration and FFTs

The equations of motion that we derived in section 3.2 form a coupled set of differential equations to

which there is no known solution. Consequently, we must numerically integrate these equations to get trajectories, which we accomplish using Runge-Kutta scheme (RK-8), numerically finding the magnetic torque at each timestep. For the chaotic study, we measure only the conservative versions of the equation of motion ($C_d = 0, \tau_c = 0$). This is because the conservative equations better represent the underlying dynamics of the magnetic coupling rather than reflecting irregularities that may occur in a highly dissipative system. While this is computationally intensive, it allows for clean chaos measurements.

3.7 Chaos Analysis

The modal analysis in the previous section describes the cradle in only the small-amplitude limit, where the motion can be described as a superposition of normal modes and is entirely regular. The question this work aims to investigate is what happens when the pendula are released from larger displacements where the magnetic coupling is strongly non-linear.

3.7.1 Phase-space portraits

We can plot the "phase-space" of a single pendulum by looking at its values of θ and $\dot{\theta}$, and tracking these evolutions over time. Regular, periodic motion returns to the same state repeatedly, while chaotic motion produces irregular results [8]. We test how the phase-space portrait jumps between N=1 magnet, and N=5 magnets. This spans a wide-range of magnetic coupling and thereby reflects the true behavior of the system.

Phase-space portraits thereby serve as a preliminary qualitative diagnostic of chaos in the system, based solely on the theoretical equations of motion.

3.7.2 Maximum Lyapunov Exponent

In order to quantify chaos, we use the Maximum Lyapunov exponent, which measures how sensitive the system is to initial conditions by quantifying how much trajectories diverge [1]. In a chaotic system, two trajectories which are close in phase-space will have a separation that grows as:

$$|\delta(t)| \approx |\delta_0| e^{\lambda t}$$

This is exponential growth, and the number that defines it is λ, or the Lyapunov exponent. Rosenstein's algorithm is used to measure the Lyapunov Exponent experimentally:

2026 S.T. Yau High School Science Award 仅用于2026丘成桐中学科学奖论文公示

$$\lambda = \lim_{|t|\to\infty} \lim_{|\delta_0|\to 0} \frac{1}{t} \ln \frac{|\delta(t)|}{|\delta_0|}$$

Rosenstein's algorithm finds an initial pair of points which are neighbors in phase-space, and follows each such pair forward in time and records how their separation grows. The logarithm of this separation is averaged over many such pairs to give the mean curve $\langle \ln | \delta(t) | \rangle$ as a function of time. The Lyapunov exponent is the slope of the best-fit line on this curve.

This is compared to the theoretical Lyapunov (where we use the damped and non-conservative equations of motion), where the same algorithm is used. However, a damped system loses energy and will always come to rest, so calculating the Lyapunov exponent over the full time frame would always be zero. To combat this, across both the theoretical and Lyapunov exponents, we only measure the initial 1.5 seconds, thereby giving us a measure of transient chaos in the system. In order to see how chaos depends on the number of magnets in the system, we test this independently for many different values of N.

4 Results

4.1 Frequency Analysis (FFT)

The tracked angle signal $\theta_j(t)$ for each magnet was converted to the frequency domain using a fast Fourier Transform (FFT). In the FFT, each normal mode contributes a sinusoidal curve oscillating at a fixed frequency and thus are seen as the peaks of a graph. The same FFT was applied to trajectories computed from the RK8 integrator, allowing us to compare theory and experiment. The uncertainty in these measurements is equal to the half-bin uncertainty of the FFT. For a time resolution of five seconds, the $\Delta f = 1/T = 1/5 = 0.2$ Hz, and therefore the half bin uncertainty is $\pm\Delta f/2 = \pm 0.1$ Hz.

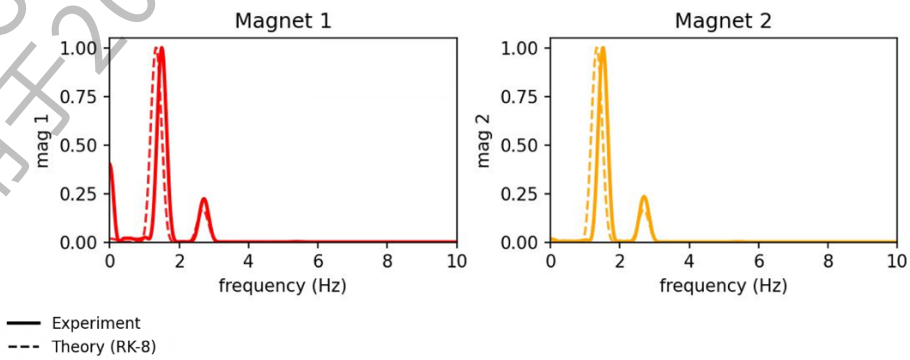


Fig. 7 – 2 Magnet FFT (Dashed lines = theory, solid lines = experiment)

2026 S.T. Yau High School Science Award
仅用于2026丘成桐中学科学奖公示

This FFT shows us the two-magnet regime, where the transforms of both magnets' angular trajectories look roughly the same. In these two graphs, the two peaks correspond to the in-phase and out-of-phase modes respectively. Note the strong fit between theory and experiment. We can also extend the FFT for the 5-magnet regime to get the following result:

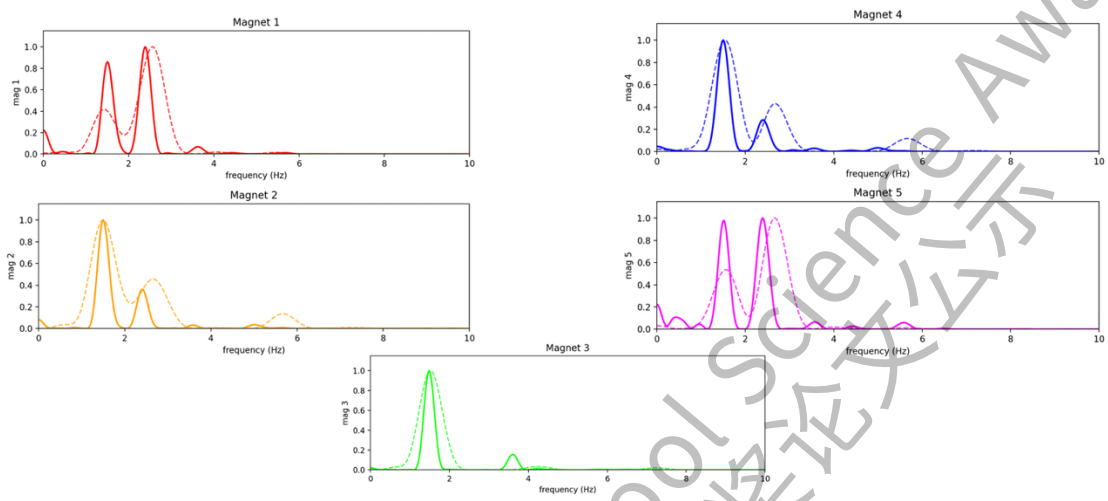


Fig. 8 – 5 Magnet FFT (Dashed lines = theory, solid lines = experiment)

This regime shows us more interesting results. For a system with N coupled oscillators, we would expect to see N normal modes. However, due to the strong effects of damping on this system, higher frequency modes which are higher energy and dissipate much faster are not seen within the resolution window of the FFT. Notably, there is a symmetry in the modes, as magnets 1 and 5 (the edge magnets), share similar graphs, as do magnets 2 and 4. The central magnet has an entirely different FFT, and the largest peak corresponds to the two centrosymmetric modes, where the central magnet is roughly stationary, while the magnets to its left and right move continuously. T

We attribute the error between the theoretical and experimental plots of the FFTs to errors in the release mechanism, as this changes the initial energy configuration of the cradle which in turn excites modes at different amplitudes and frequencies.

To verify our analytical closed-form model, we compare our analytical frequencies (derived from the eigenvalue problem in section 3.5) to those we measured experimentally and numerically:

2026 S.T. Yau High School Science Award
仅用于2026丘成桐中学科学奖论文公示

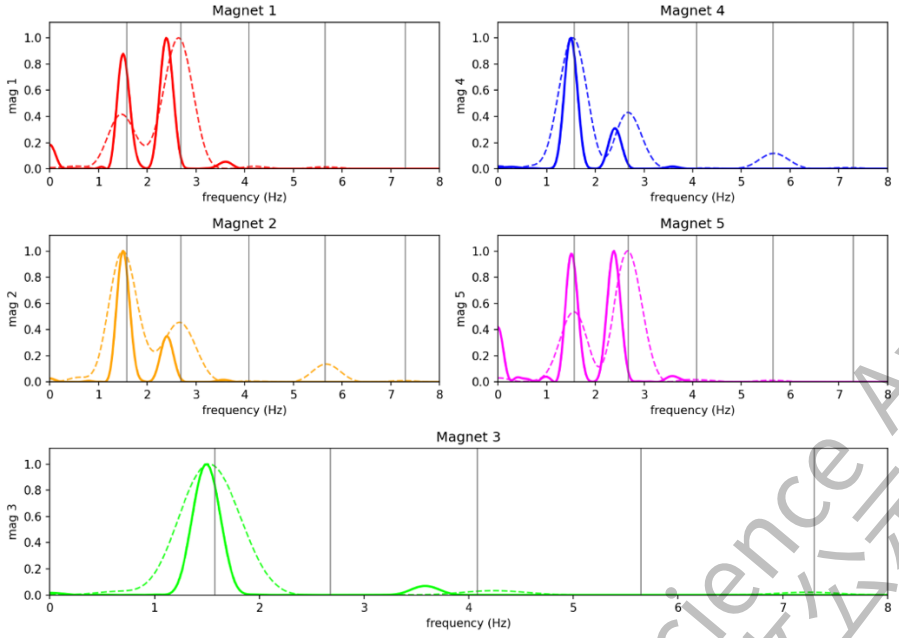


Fig. 9 – Vertical lines represent predicted analytical frequencies.

4.2 Parameter Dependence

To test the model beyond a single configuration, the mode frequencies were computed analytically while varying the remanent flux density B_r, the pivot spacing a, and the pendulum length l. The analytical theory is given by the dashed line. We only plot these for the first three modes, as these are the only ones which are experimentally visible.

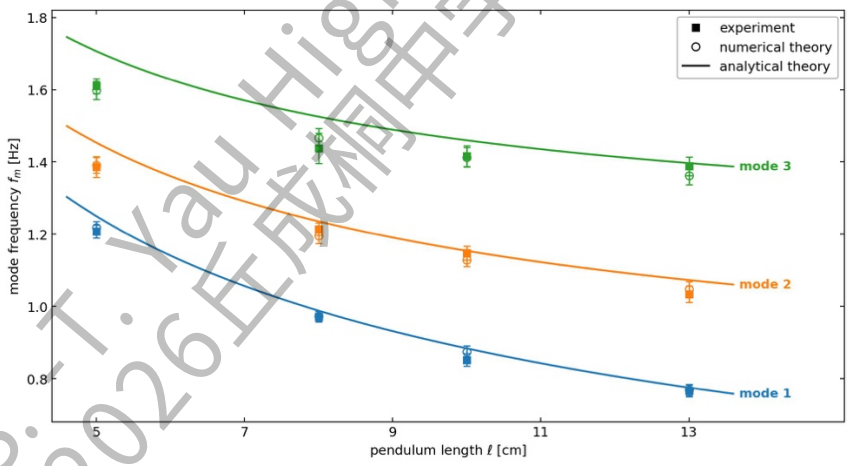


Fig. 10 - Mode Frequencies vs. Pendulum Length

This graph fits with our physical intuition, as increasing the length of the pendulum raises the moment of inertia and thus reduces the strength of each mode. All three modes fall together within the measured range, although there are deviations at lower error. We hypothesize that this is because our constant frictional torque assumption breaks down at shorter pendulums.

2026 S.T. Yau High School Science Award 仅用于2026丘成桐中学科学奖论文公示

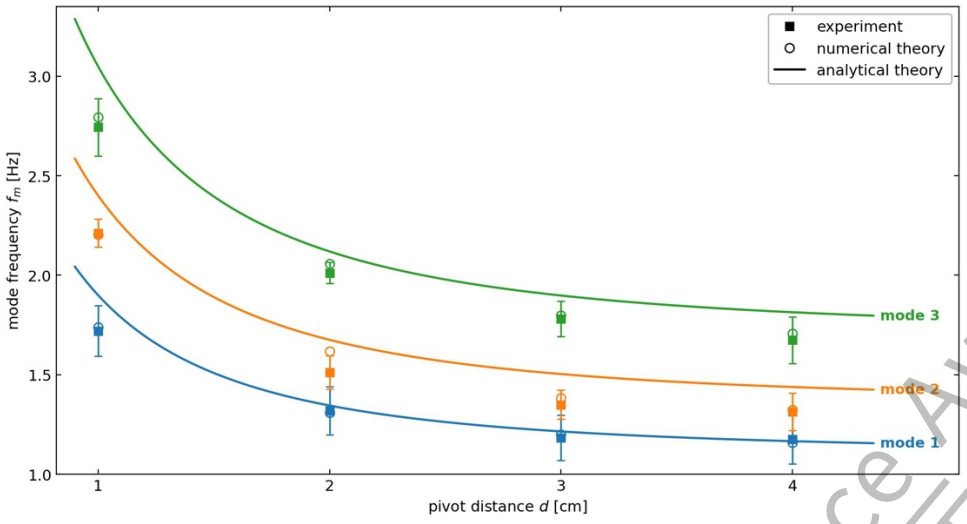


Fig. 11 - Mode frequency vs. pivot distance

Testing the numerical and analytical theories for pivot distance as well yields reasonable fit, although the analytical theory overpredicts both the experiment and numerical theories. We believe this is because the Furlani model assumes perfectly co-axial with straight line separation, but as the separation distance decreases, even small swings produce large lateral offsets which reduce the accuracy of the model. By contrast, the numerical theory, which uses the surface currents model, works for all distances and therefore does not face this issue.

The last parameter we varied was the B_r. The results are shown below:

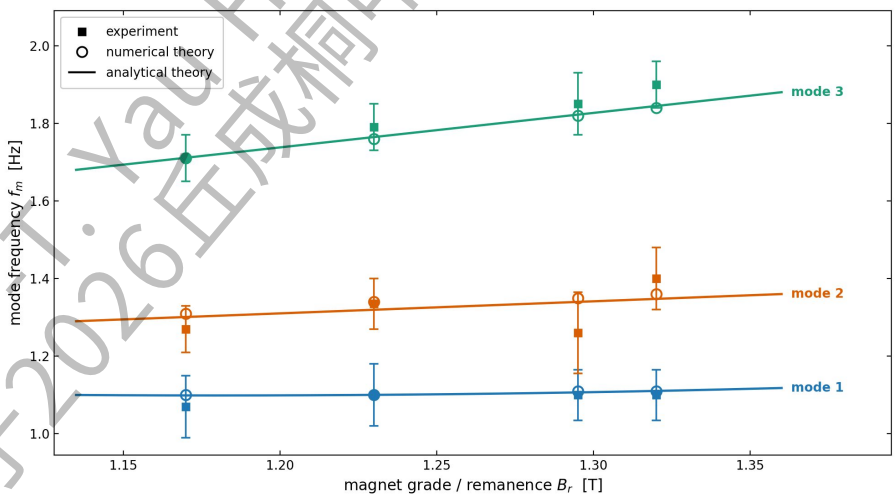


Fig. 12 – Mode frequency vs. Magnetic Remanence (Different magnet grades)

By varying the 4 different neodymium magnets, we can see that higher remanences produce higher mode frequencies. Increasing magnet strength leads to stronger repulsion and thereby stiffer coupling. Notably, the higher modes are more strongly affected, and this could be because they involve more relative moment

2026 S.T. Yau High School Science Award
仅用于2026丘成桐中学科学奖论文公示

between neighbors and thus magnetic stiffness plays a larger role.

4.3 Phase-space

The character of the motion is most directly shown through the phase-space of the system. The conservative phase-space plots will differ from those that are damped, as the damped versions will always collapse onto a fixed point when the motion stops. The conservative 1-magnet regime has the following phase-space:

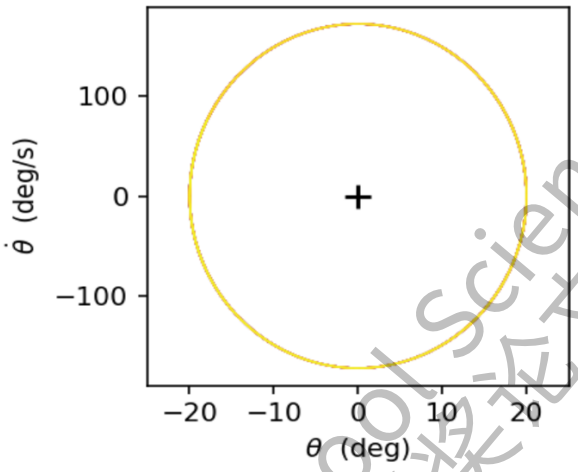


Fig. 13 - Theoretical Phase Space of 1-magnet regime (conservative)

This trajectory forms an integrable and direct closed loop. With no neighboring magnets there is no magnetic coupling, and thus the system behaves exactly like a simple pendulum in the ideal condition. By comparison, the same technique, when applied to the five magnet-regime, produces the following:

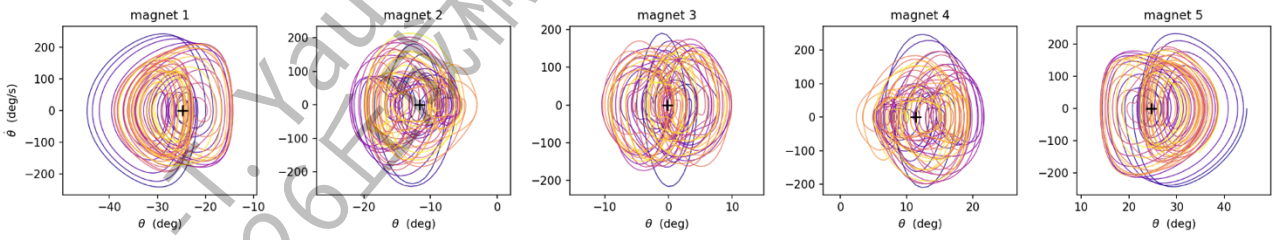


Fig. 14- Theoretical Phase Space of 5-magnet regime (conservative)

The trajectory of each magnet is no longer a closed loop but is instead densely filled and aperiodic. Each portrait is a project of the full ten-dimensional phase-space trajectory, and the trajectory moves around on a constant-energy surface without repeating. This qualitatively signals that the system is chaotic. We conduct this quantitatively in the next section.

4.4 Lyapunov Exponent

2026 S.T. Yau High School Science Award 仅用于2026丘成桐中学科学奖论文公示

Following the method of section 3.6, the mean logarithmic separation between initially neighboring trajectories was computed by Rosenstein's algorithm and plotted against time.

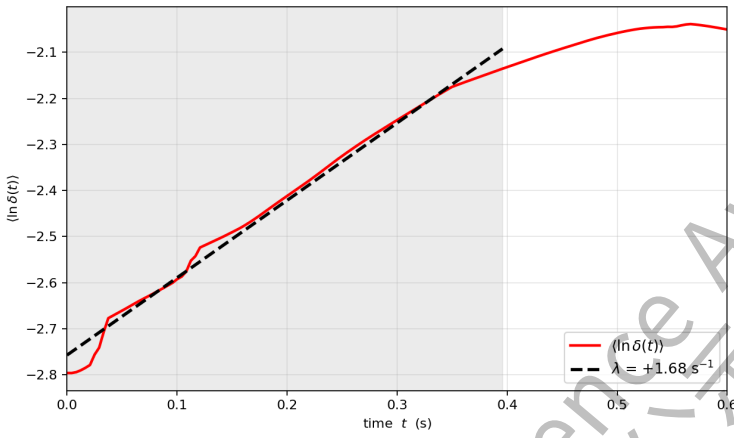


Fig 15. - Log separation of trajectories over time

Notice that the that the linear section of the curve (the part responsible for chaos), exists only in the first 0.4 seconds. This shows us that the system exhibits *transient chaos*. A Maximum Lyapunov exponent greater than zero indicates that the system is chaotic. With an experimental value of $\lambda = 1.68\frac{1}{s}$, this quantifiably signals that the system exhibits chaotic behavior. Our theoretical value, with a trajectory numerically integrated and then calculated using the same method, has a value of $\lambda = 1.73\frac{1}{s}$.

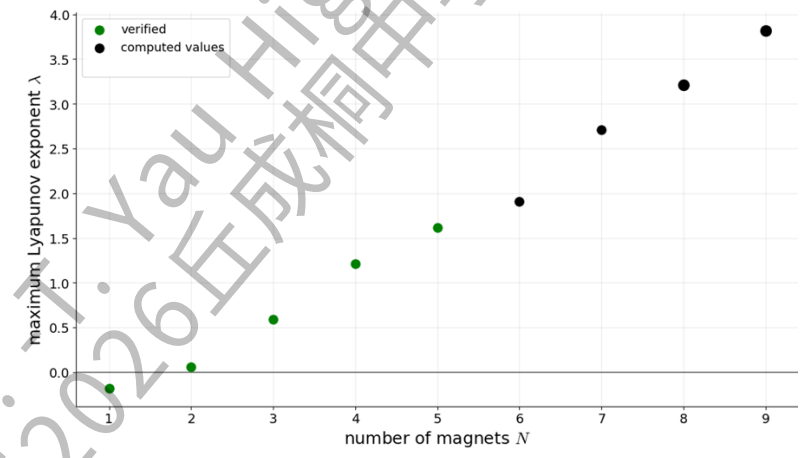


Fig 16. - Lyapunov Exponent vs. Number of magnets

In order to show descent into chaos, we experimentally find the MLE for each of N=1 through N=5 magnets, and compute theoretically for N=6, 7, 8, and 9. We see that the MLE for N=1 is negative, as this corresponds to the system being a highly damped oscillator. As the number of magnets increases, it is evident that chaotic behavior in the system also increases. We do **not** claim that this relationship is linear, as the MLE is a discrete and dynamic value that cannot be interpolated. However, we can say conclusively

2026 S.T. Yau High School Science Award 仅用于2026丘成桐中学科学奖论文公示

that increased magnetic coupling leads to a higher degree of trajectory divergence, and thus chaos.

5 Limitations and Scope

While our experimental setup was highly controlled and reproducible, one area in which it could be improved is through the hand release. Specific initial angles were calibrated using a protractor, but the release mechanism was still by hand. This may contribute to deviations between theory and experiment, specifically for the variation of different parameters, although we believe these effects are not as significant. Another limitation is that the damping coefficients were measured once and then assumed to be held constant across all different configurations. However, in practice, it is likely that axle friction varies with pendulum length, which could also have led to errors. In measuring the transient chaos, only the first second dominated most of the chaotic behavior, and because this initial regime is noisy, this could have impacted the validity of the computed MLEs. An automated release mechanism would be an ideal extension to this work. Finally, the chain could be pushed experimentally to larger values of N to more closely and accurately model the systems descent into chaos as N increases, perhaps studying soliton or wave packet behavior.

6 Conclusion

This work has studied the Magnetic Newton's Cradle as a one-dimensional chain of coupled non-linear oscillators. We have a built a mechanical form for the system, using the Furlani force for closed-form analysis and the surface-currents model for more general numerical integration. We have constructed a novel and highly precise experimental setup, varied multiple parameters to understand behavior dependence, and shown that our theory and data have good fit. We used FFTs to conduct frequency analysis, broke down the systems into its normal modes, and discussed chaotic behavior in the system. We believe this work sheds light on specific systems of magnetically coupled oscillators, and this work can be extended to study larger and more general chaotic regimes.

2026 S.-T. Yau High School Science Award
仅用于2026丘成桐中学科学奖论文公示

7 References

1. Rosenstein, M. T., Collins, J. J., & De Luca, C. J. (1993). A practical method for calculating largest Lyapunov exponents from small data sets. *Physica D: Nonlinear Phenomena, 65*(1–2), 117–134. https://doi.org/10.1016/0167-2789(93)90009-P
2. Savitzky, A., & Golay, M. J. E. (1964). Smoothing and differentiation of data by simplified least squares procedures. *Analytical Chemistry, 36*(8), 1627–1639. https://doi.org/10.1021/ac60214a047
3. Shinbrot, T., Grebogi, C., Wisdom, J., & Yorke, J. A. (1992). Chaos in a double pendulum. *American Journal of Physics, 60*(6), 491–499. https://doi.org/10.1119/1.16860
4. Furlani, E. P. (2001). *Permanent Magnet and Electromechanical Devices: Materials, Analysis, and Applications*. Academic Press. https://doi.org/10.1016/B978-0-12-269951-1.X5000-1
5. Ravaud, R., Lemarquand, G., Babic, S., Lemarquand, V., & Akyel, C. (2010). Cylindrical magnets and coils: Fields, forces, and inductances. *IEEE Transactions on Magnetics, 46*(9), 3585–3590. https://doi.org/10.1109/TMAG.2010.2049026
6. Vučković, A. N., Perić, M. T., Ilić, S. S., Raičević, N. B., & Vučković, D. M. (2021). Interaction magnetic force of cuboidal permanent magnet and soft magnetic bar using hybrid boundary element method. *ACES Journal, 36*(11), 1492–1498. https://doi.org/10.13052/2021.ACES.J.361114
7. Vokoun, D., Beleggia, M., Heller, L., & Šittner, P. (2009). Magnetostatic interactions and forces between cylindrical permanent magnets. *Journal of Magnetism and Magnetic Materials, 321*(22), 3758–3763. https://doi.org/10.1016/j.jmmm.2009.07.030
8. Strogatz, S. H. (2015). *Nonlinear Dynamics and Chaos: With Applications to Physics, Biology, Chemistry, and Engineering* (2nd ed.). Westview Press.
9. Peitgen, H.-O., Jürgens, H., & Saupe, D. (1992). *Chaos and Fractals: New Frontiers of Science*. Springer. https://doi.org/10.1007/978-1-4757-4740-9
10. Christian, J. M., & Middleton-Spencer, H. A. J. (2020). Chaos in the magnetic pendulum. *Mathematics Today*, April 2020, 70–74.
11. Qin, B., & Zhang, Y. (2024). Comprehensive analysis of the mechanism of sensitivity to initial conditions and fractal basins of attraction in a novel variable-distance magnetic pendulum. *Chaos, Solitons & Fractals, 183*, 114933. https://doi.org/10.1016/j.chaos.2024.114933
12. Bradski, G. (2000). The OpenCV Library. *Dr. Dobb's Journal of Software Tools, 25*(11), 120, 122–125.
13. Cooley, J. W., & Tukey, J. W. (1965). An algorithm for the machine calculation of complex Fourier series. *Mathematics of Computation, 19*(90), 297–301. https://doi.org/10.1090/S0025-5718-1965-0178586-1
14. Georgi, H. (1993). *The Physics of Waves*. Prentice Hall.
15. Cline, D. (2019). *Variational Principles in Classical Mechanics* (Rev. 2nd ed.). University of Rochester, River Campus Libraries. https://doi.org/10.16925/bov1.

2026 S.T. Yau High School Science Award 仅用于2026丘成桐中学科学奖论文公示

16. Torre, C. G. (2014). Linear chain of coupled oscillators. *Foundations of Wave Phenomena*, Paper 19. Utah State University. https://digitalcommons.usu.edu/foundation_wave/19/
17. Ashcroft, N. W., & Mermin, N. D. (1976). *Solid State Physics*. Holt, Rinehart and Winston.

8 Appendix

8.1 Link to demonstrative experimental videos - https://drive.google.com/drive/folders/1A6AOmWefCXb1mlNUuY9gLlgu5zbSc1Sb?usp=sharing

2026 S.-T. Yau High School Science Award
仅用于2026丘成桐中学科学奖论文公示